Radiation Dosimetry of a Clinical Prototype Dedicated Cone-beam Breast CT System with Offset Detector

Hsin Wu Tseng[1], Andrew Karellas[1] and Srinivasan Vedantham[1, 2, *]

[1]Department of Medical Imaging, The University of Arizona, Tucson, AZ

[2]Department of Biomedical Engineering, The University of Arizona, Tucson, AZ

*Corresponding author

Contact information:

Srinivasan Vedantham, PhD, DABR, FAAPM
Professor, Medical Imaging (DMI) and Biomedical Engineering (BME)
The University of Arizona
1501 N Campbell Ave, PO Box 245067
Tucson, AZ 85724-5067.
Telephone: (520) 626-6641
Fax: (520) 626-2643
E-mail: svedantham@radiology.arizona.edu

Abstract

Purpose: A clinical prototype dedicated cone-beam breast computed tomography (CBBCT) system with offset-detector is undergoing clinical evaluation at our institution. This study is to estimate the normalized glandular dose coefficients (DgN^{CT}) that provide air-kerma to mean glandular dose conversion factors using Monte Carlo simulations.

Materials and Methods: The clinical prototype CBBCT system uses 49 kV x-ray spectrum with 1.39 mm 1st half-value layer thickness. Monte Carlo simulations (GATE, version 8) were performed with semi-ellipsoidal, homogeneous breasts of various fibroglandular weight fractions ($f_g = 0.01, 0.15, 0.5, 1$), chest-wall diameters ($d = 8, 10, 14, 18, 20$ cm) and chest-wall to nipple length ($l = 0.75d$), aligned with the axis of rotation (AOR) located at 65 cm from the focal spot to determine the DgN^{CT}. Three geometries were considered – 40×30-cm detector with no offset that served as reference and corresponds to a clinical CBBCT system, 30×30-cm detector with 5 cm offset, and a 30×30-cm detector with 10 cm offset.

Results: For 5 cm lateral offset, the DgN^{CT} ranged $0.177 - 0.574$ mGy/mGy and reduction in DgN^{CT} with respect to reference geometry were observed only for 18 cm ($6.4\% \pm 0.23\%$) and 20 cm ($9.6\% \pm 0.22\%$) diameter breasts. For the 10 cm lateral offset, the DgN^{CT} ranged $0.221 - 0.581$ mGy/mGy and reduction in DgN^{CT} with were observed for all breast diameters. The reduction in DgN^{CT} were $1.4\% \pm 0.48\%$, $7.1\% \pm 0.13\%$, $17.5\% \pm 0.19\%$, $25.1\% \pm 0.15\%$, and $27.7\% \pm 0.08\%$ for 8, 10, 14, 18 and 20 cm diameter breasts, respectively. For a given breast diameter, the reduction in DgN^{CT} with offset detector geometries were not dependent on f_g. Numerical fits of $DgN^{CT}(d, l, f_g)$ were generated for each geometry.

Conclusion: The DgN^{CT} and the numerical fit, $DgN^{CT}(d, l, f_g)$ would be of benefit for current CBBCT systems using the reference geometry and for future generations using offset-detector geometry. There exists a potential for radiation dose reduction with offset-detector geometry, provided the same technique factors as the reference geometry are used, and the image quality is clinically acceptable.

Keywords: Breast cancer, Breast CT, Radiation dose, Mean Glandular Dose, Offset detector, Truncated detector, Monte Carlo.

1. Introduction

The clinical potential of dedicated breast computed tomography (BCT) is being investigated by several research teams[1-17] and topical reviews have been published[18-21]. The motivation for pursuing BCT is its ability to provide fully tomographic images in comparison to partial tomographic images provided by digital breast tomosynthesis[22,23], which results in artifacts[24,25]. Broadly, dedicated BCT designs can be classified as those using helical acquisition[15] similar to multi-detector CT, or as cone-beam breast CT (CBBCT) with planar detectors and circular scan trajectory[2,3]. The planar detectors used in most CBBCT systems are amorphous silicon-based flat-panel imagers[26] with 40×30 cm field-of-view (FOV) and are operated in 0.388 mm pixel pitch. In a diagnostic setting, non-contrast CBBCT with one system (KBCT1000, Koning Corp., West Henrietta, NY, USA) has shown improved sensitivity compared to mammography.[9] The mean glandular dose (MGD) to the breast from diagnostic non-contrast CBBCT exam using one clinical prototype CBBCT system is approximately twice that of a screening mammogram.[27] When the MGD from the CBBCT exam is reduced to screening mammography levels, the conspicuity of calcifications is lower than mammography[28] due to the relatively high system noise[29] from the flat-panel detector.

Complementary Metal Oxide Semiconductor (CMOS) detectors[30] provide for smaller pixel pitch (0.075 – 0.15 mm), high-frame rate operation (>30 frames/s without pixel binning) and exhibit approximately 10-fold reduction in electronic noise[31]. The detector also has reduced dead-space at the chest-wall (15 mm) compared to the 40×30 cm detector (26 mm) used in current United States Food and Drug Administration (US FDA)-approved clinical CBBCT system, which can improve posterior coverage[32]. However, the largest FOV among currently available CMOS detectors is 30×30 cm. A clinical prototype dedicated CBBCT with offset-detector geometry was designed[33,34] and developed at our institution in collaboration with the industry (Koning Corp., West Henrietta, NY, USA). This system has been fabricated and installed in the breast imaging facility for clinical evaluation. A clinical trial (ClinicalTrials.gov identifier: NCT03954431) to evaluate this system is to begin soon and if successful, could result in clinical systems based on this design. The concept of offset-detector geometry for CBBCT was previously investigated using bench-top setups[35,36]. The study by McKinley et al.[35] used a flat-panel detector with 1920x1536 pixels of 127 µm pitch, resulting in a detector FOV of 24.4×15.7 cm. The study used detector pixel binning and ordered subsets transmission (OS-TR) iterative algorithm to provide approximately 1 mm voxels, and demonstrated the ability to obtain reconstructed images without truncation artifacts using phantoms[35]. The study by Mettivier et al.[36] showed a reduction in cupping artifacts due to reduced x-ray scatter contribution arising from partial irradiation. While the above studies demonstrate feasibility of the offset-detector geometry for CBBCT, the focus of this work is on a clinical prototype system suitable for patient imaging.

An important component of the CBBCT system evaluation is the radiation dosimetry. Radiation dosimetry for CBBCT with circular[37-40], saddle[10] and circle-plus-line[41] x-ray source trajectories have been published. Although the installed CBBCT prototype uses circular, full-scan (360°) x-ray source trajectory, the offset-detector geometry results in partial irradiation of the breast in each view. The proportion of breast volume irradiated by the primary x-ray beam is dependent on breast dimensions. Thus, the purpose of the study is to estimate the air kerma-to-mean glandular dose (MGD) conversion factors, also referred to as normalized glandular dose coefficients (DgN^{CT}) appropriate for this geometry using Monte Carlo simulations. Also, the reduction in DgN^{CT} with the offset-detector geometry was quantified with respect to the clinical system (KBCT 1000, Koning Corp.) with no detector offset. A

preliminary study[42] was presented at the annual meeting of the American Association of Physicists in Medicine (AAPM). We followed the reporting guidelines recommended by the Task Group No. 268 of the AAPM.[43]

2. Materials and Methods

2.1. Offset detector CBBCT prototype

Fig 1. Photograph of the dedicated cone-beam breast CT system employing offset detector geometry.

The CBBCT prototype system (Fig 1) installed in our institution uses a high-power (12 kW), "flipped" anode x-ray tube[44] with 0.3 mm nominal focal spot (M1583, Varex Imaging, Salt Lake City, UT, USA) operating in pulsed mode (8 ms pulse-width) and is powered by a high-frequency x-ray generator (Sedecal USA Inc., Buffalo Grove, IL, USA) The source-to-detector distance (SDD) is 898 mm and the source-to-axis of rotation (AOR) distance is 650 mm. The system is configured to operate at 49 kV and the 1st half-value layer thickness (HVT) is 1.39 mm of Al. The exposure at isocenter was measured using an exposure meter (MDH 1515, Radcal Corp., Monrovia, CA, USA) and an ionization chamber (Model 10x5-6, Radcal Corp., Monrovia, CA, USA) over the tube current range of 12 to 125 mA. The measured exposure was converted to air kerma using a conversion factor of 8.73 mGy/R. A 30×30 cm CMOS detector (Xineos 3030HS, Teledyne-Dalsa, Waterloo, ON, Canada) operated at 30 frames/s and 0.152 mm pixel pitch is used for image acquisition. In order to compensate for the smaller FOV of the CMOS detector, an offset detector geometry is employed. The detector mount allows for either a 5 cm or a 10 cm lateral offset. A 5 cm lateral offset of the 30×30 cm detector extends the FOV to 40×30 cm matching the FOV of a clinical CBBCT system, and a 10 cm offset extends it to 50×30 cm. The extended FOV could be of benefit for evaluating the lymph nodes in the lower axillary region[3], but needs to be demonstrated through a clinical trial. Evaluation of reconstruction algorithms appropriate for this geometry is in progress.[33,35,45]

2.2. Breast model

The uncompressed breast in pendant geometry was modeled as a semi-ellipsoid in shape with minor axis corresponding to the radius of the breast at the chest-wall (r) and the major axis corresponding to the chest-wall to nipple length (l). Clinical studies indicate that the effective diameter of the breast at the chest-wall ranges 8–20 cm, with median (1st quartile, 3rd quartile) of approximately 14 cm (10 cm, 18 cm).[46,47] Hence, the diameter ($d = 2r$) of the semi-ellipsoidal breast at the chest-wall were chosen from $d \in \{8, 10, 14, 10, 20\}$ cm. For the selected d, the chest-wall to nipple length was set to $l = 0.75d$. This is a reasonable approximation of $l = 0.7d$ observed in a clinical study[47]. The skin thickness comprising the epidermis and dermis was chosen to be 1.45 mm based on prior literature [48,49]. The breast parenchyma was modeled as a homogenous mixture of adipose and fibroglandular tissues with fibroglandular weight fraction (f_g) of 0.1, 0.15, 0.5, 0.75 and 1. Traditionally, $f_g = 0.5$ had been used in the United States to represent the "average" breast composition.[50] However, clinical studies[47,51] indicate that the $f_g \approx 0.15$. Elemental compositions for adipose, fibroglandular and skin tissues reported by Hammerstein *et al*. were used.[52]

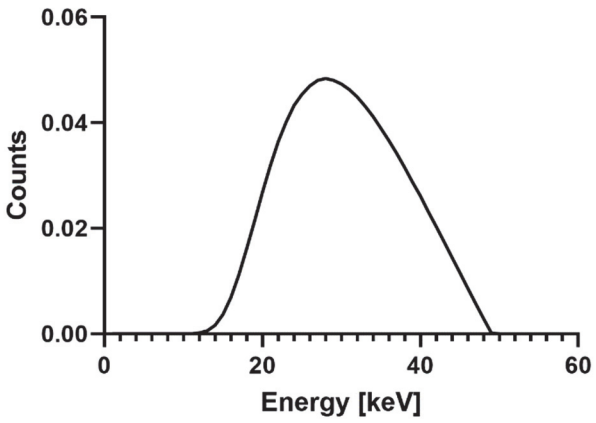

Fig 2. Tungsten-anode 49 KV x-ray spectrum (1st HVT: 1.39 mm of Al, mean energy: 30.4 keV) normalized to unit area.

2.3. Monte Carlo simulations

An open-source, Monte Carlo simulation tool[53,54] (GEANT4 Application for Tomographic Emission, GATE version 8.0) was used for radiation transport. A tungsten-target, 49 kV x-ray spectrum[55] with added aluminum filter was modeled to achieve a 1st HVT of 1.39 mm of Al. Fig 2 shows the x-ray spectrum normalized to unit area. The semi-ellipsoidal homogenous breast was aligned with the AOR, which is at 650 mm from the source. Fig 3 shows the simulation geometry for the 3 combinations of detectors and lateral offset. Simulations were performed using the low energy physics package. The simulation consisted of a 0.3 mm × 0.3 mm x-ray focal spot, which emitted x-ray photons towards the breast located at a distance of 650 mm. The direction of the x-ray photons emitted from the focal spot was

random and was restricted so that all x-ray photons are directed towards the detector located at 898 mm from the x-ray source and were incident on the breast. The energy of the x-ray photon was sampled from the spectrum shown in Fig 2. Independent studies by Sechopoulos *et al.*[39] and Vedantham *et al.*[41] used 10^6 x-ray photons and achieved a coefficient of variation (COV) of less than 0.7%. Hence, 10^6 x-ray photons were used in our Monte Carlo simulations. For the offset detector geometries considered, the COV was determined from 5 Monte Carlo runs with the smallest diameter breast ($d = 8$ cm, $l = 6$ cm, and $f_g = 0.01$). The normalized glandular dose (DgN^{CT}) (mGy/mGy) can be computed as[21,24]

$$DgN^{CT}_{homogeneous} = \frac{\sum_m E_{dep} G(f_g,E)}{f_g m \sum_E \Phi(E)\Theta(E)} \quad (1)$$

where E_{dep} is the energy deposited within the breast of mass m, f_g is the fibroglandular weight fraction, $\Phi(E)$ and $\Theta(E)$ are the x-ray fluence and the fluence-to-air kerma (AK) conversion factor at energy, E, respectively. $G(f_g,E)$ apportions the total energy deposited in the breast to the radiation-sensitive fibroglandular tissue[26]

$$G(f_g,E) = \frac{f_g[\mu_{en,g}(E)/\rho_g]}{f_g[\mu_{en,g}(E)/\rho_g]+(1-f_g)[\mu_{en,a}(E)/\rho_a]} \quad (2)$$

where $\mu_{en,g}(E)$ and $\mu_{en,a}(E)$ are the energy-dependent, mass-energy absorption coefficients of fibroglandular and adipose tissues, and, ρ_g and ρ_a are the mass densities of fibroglandular and adipose tissues, respectively. All Monte Carlo simulations were performed using a Dell workstation 7810 with Intel Xeon CPU (3.20 GHz) and 32 GB RAM and took approximately 40 minutes per simulation.

2.4. Validation of Monte Carlo simulations

Sechopoulos *et al.*[39] used the GEANT4 toolkit (version 9.3) to determine the normalized glandular dose conversion factors, DgN^{CT}, for a CBBCT system with identical geometry and x-ray spectrum and validated the simulations with experimental measurements. This system was the prototype version (prior to FDA approval) of KBCT1000 and used a 40×30 cm detector with no lateral offset. We refer to this as the "reference" geometry. The study by Sechopoulos *et al.*[39] reported DgN^{CT} for 10–18 cm diameter breasts. A subsequent study[27] numerically fitted these DgN^{CT} values so that it can be extended for 8–20 cm diameter breasts and the fit equation provided was:

$$DgN^{CT}_{Fit} = \left[1.0758247 - 0.2353669 \times \ln(d) - 0.1253462 f_g\right] \times \left[0.1153 \times \ln\left(\frac{l}{d}\right) + 1.0818\right] \quad (3)$$

The numerical fit was reported to be within 0.55% for the 90 values of DgN^{CT} arising from different combinations of d, l and f_g.[27] Hence, the DgN^{CT} values from the Monte Carlo simulations performed for the reference geometry in this study were validated with the data reported by Sechopoulos *et al.*[39] for 10–18 cm diameter breasts and with the numerical fit reported by Vedantham *et al.*[27] for the complete range of diameters.

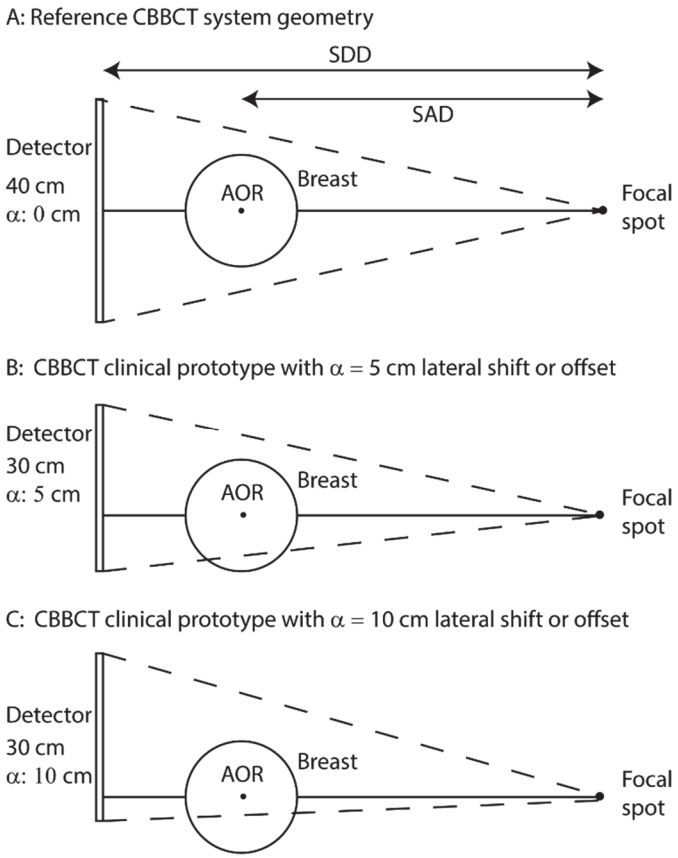

Fig 3. Imaging geometry (coronal view) for (A) the reference CBBCT system using 40×30 *cm detector with no lateral offset, (B) the offset-detector CBBCT system using* 30×30 *cm detector with* $\alpha = 5$ *cm lateral offset, and (C) the offset-detector CBBCT system using* 30×30 *cm detector with* $\alpha = 10$ *cm lateral offset. The axis-of-rotation is denoted as AOR. The AOR and detector are located at* $SAD = 65$ *cm and* $SDD = 89.8$ *cm from the source. The extent of the detector along the chest-wall to nipple direction is 30 cm and is identical in all 3 geometries (not shown). The breast is modeled as a semi-ellipsoid. A breast with 20 cm diameter at chest-wall is shown.*

2.5. Theoretical expectations

Let us consider a breast of radius (r) at the chest-wall aligned with the AOR that is located at SAD. Let r_{max} represent the largest breast diameter expected in a population. We define the center line as the projection of the AOR from the source to the detector plane located at SDD. The system magnification (M) can be defined as $M = SDD/SAD$. Let us consider a detector with lateral width W that is centered with respect to the center line. The x-ray beam is collimated so as to irradiate only the detector. This corresponds to the reference geometry mentioned above, as the detector is not laterally shifted, i.e., detector lateral offset is zero. If the detector lateral width satisfies $W \geq M\ 2r_{max}$, then the entire breast volume is irradiated by the primary beam and the projection of the entire breast will be captured by the detector. For the current clinical CBBCT system (KBCT1000), this condition is satisfied. The largest breast diameter reported is $2r_{max} = 20.5$ cm. The system magnification is $M = 898/650 = 1.382$. The 40 cm

lateral extent of the PaxScan 4030 (Varex Imaging, Salt Lake City, UT, USA) detector satisfies this condition as it exceeds $M\ 2r_{max} = 28.3$ cm.

Let us now consider the detector of lateral width W that is laterally-shifted and this shift or offset is denoted as α. For convenience, let us define half-detector width $H = \frac{W}{2}$. At SDD, the detector extent is $[H + \alpha, H - \alpha]$. Scaling it to the AOR, the detector extent is $\left[\frac{H+\alpha}{M}, \frac{H-\alpha}{M}\right]$. Then, the entire breast volume will be irradiated by the primary beam only if, $r \leq \frac{H-\alpha}{M}$. Rewriting this in terms of diameter (d) of the breast at the chest-wall and lateral width (W) of detector yields,

$$d \leq (W - 2\alpha)/M \tag{4}$$

Thus, the theoretical expectation is that when the above inequality is satisfied the DgN^{CT} from offset-detector geometry should not be different from the reference geometry. Also, when d exceeds $(W - 2\alpha)/M$, (i) the DgN^{CT} for offset-detector geometry will be smaller than the reference geometry due to partial irradiation of the breast volume, and (ii) the differences in DgN^{CT} between offset and reference geometries will increase with breast diameter, as the proportion of the breast volume irradiated by the primary beam decreases. In order to quantify the change in DgN^{CT} between offset-detector and reference geometries when $d > (W - 2\alpha)/M$, the percent reduction in DgN^{CT} was computed as,

$$\%\ \text{Reduction in}\ DgN^{CT} = \left(1 - \frac{DgN^{CT}[\text{offset geometry}]}{DgN^{CT}[\text{reference geometry}]}\right) \times 100 \tag{5}$$

For the 30×30 cm detector (Xineos 3030HS, Teledyne-Dalsa, Waterloo, ON) with 5 cm lateral offset, breasts with diameters $d > 14.48$ cm will be partially irradiated. Since $d = 14.48$ cm approximates the median breast diameter reported in literature, the DgN^{CT} provided in this study will be applicable to approximately half of the population who undergo CBBCT exam using this offset-detector geometry.

For the 30×30 cm detector with 10 cm lateral offset, breasts with diameters exceeding 7.24 cm will be partially irradiated. Since $d = 7.24$ cm is smaller than the minimum breast diameter reported in literature, the DgN^{CT} provided in this study will be applicable to all women who undergo CBBCT exam using the 10 cm lateral offset-detector geometry.

2.6. Data analysis

All data analyses were performed using statistical software (SAS® version 9.4, SAS Institute Inc., Cary, NC, USA). Linear regression analyses were used to validate the DgN^{CT} from this study with prior reports. The intercepts from the regression analyses were tested to determine if they differ significantly from zero. The 95% confidence intervals for the slopes were used to determine if they span unity. The residuals were tested for normality assumption (Shapiro-Wilks test). Depending on the results from the normality tests, one sample t-test or median test was used to determine if the residuals significantly differed from zero.

For the reference geometry, Sechopoulos et al reported DgN^{CT} for 90 combinations of d, l and f_g spanning 10 – 18 cm diameter breasts. Since this study provided additional data for 8 cm and 20 cm breasts as well as for $f_g = 0.15$, the two datasets were combined to generate a numerical fit. This would

enable its use for current clinical CBBBCT systems. Similarly, numerical fits were generated for the two offset-detector geometries. This could be useful for our current CBBCT prototype and potentially for future clinical CBBCT systems. Separate numerical fits were generated for each of the 3 imaging geometries. First, the optimal transforms of the independent variables (d, l and f_g) were determined using transformation regression. After transforming these variables, robust regression using least trimmed squares was used to obtain the weighted least square estimates. The fit coefficients obtained from robust regression were verified by linear regression analysis of the DgN^{CT} values derived from the numerical fit and that from Monte Carlo simulations.

3. Results

3.1. Air Kerma at Isocenter

Fig 4 shows the linear regression analysis of the air kerma (mGy) at isocenter and the tube current (mA). The system demonstrated a linear behavior ($r^2 = 0.9994$) and the fit equation is provided in the figure. The point estimate ± standard error of the slope and the intercept were 0.2441±0.002 and 0.0552±0.126, respectively. Since the system uses 8 ms pulse-width and 300 projections, the product of tube current and exposure duration (mAs) for the entire scan can be computed as $2.4 \times mA$.

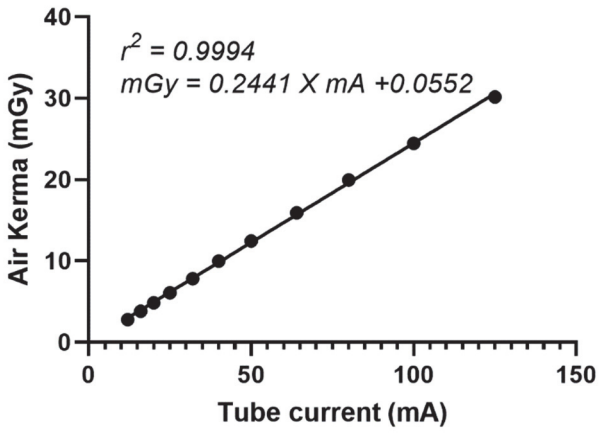

Fig 4. Linear regression of air kerma (mGy) at isocenter and tube current (mA). Each scan acquires 300 projections and the x-ray pulse-width in each projection is 8 ms.

3.2. Validation

Fig 5A shows the results from the linear regression analysis of the DgN^{CT} from this study and that reported by Sechopoulos *et al.*[39] for 10–18 cm diameter breasts. Good agreement is observed with $r^2 = 0.976$. The point estimate ± standard error of the slope and the intercept were 1.078±0.064 and -0.028±0.027, respectively. The intercept did not differ significantly from zero (p=0.168). The 95% confidence interval for the slope was $(0.928, 1.229)$ and encompassed unity. The residuals were

normally distributed (p=0.851) and did not significantly differ from zero (p=1.0). Fig 5B shows the results from the linear regression analysis of the DgN^{CT} from this study and the numerical fit provided by Vedantham *et al.*[27] for all breast diameters considered. Good agreement is observed with $r^2 = 0.988$. The point estimate ± standard error of the slope and the intercept were 0.989±0.026 and -0.011±0.012, respectively. The intercept did not significantly differ from zero (p=0.16). The 95% confidence interval for the slope was $(0.935, 1.044)$ and encompassed unity. The residuals were normally distributed (p=0.859) and did not significantly differ from zero (p=1.0). These results validate our Monte Carlo simulation framework.

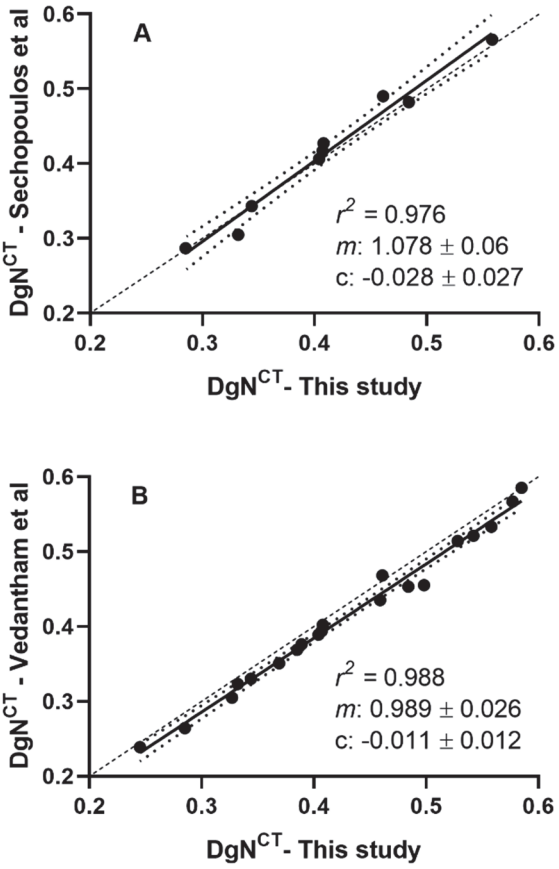

Fig 5. Validation of the Monte Carlo simulation. For the reference geometry with no detector offset, the DgN^{CT} values from the Monte Carlo simulations were validated with (A) the data reported by Sechopoulos et al.[39] for 10–18 cm diameter breasts and (B) the numerical fit reported by Vedantham et al.[27] for the complete range of diameters. Dashes represent the identity line and the dotted lines indicate the 95% confidence band. Slope and intercept are represented as m and c, respectively. In both panels, the 95% confidence interval of the slopes encompassed unity and the intercepts did not significantly differ from zero (p>0.16).

3.3. DgN^{CT} for reference CBBCT

Table 1 summarizes the DgN^{CT} values for the reference CBBCT system (KBCT1000, Koning Corp., West Henrietta, NY, USA), which uses a 40×30 cm detector with no lateral offset or shift. This table extends the DgN^{CT} values beyond the 10–18 cm diameter range to include 8 cm and 20 cm diameter breasts. Also, the table provides for an additional fibroglandular weight fraction of $f_g = 0.15$.

Table 1. DgN^{CT} for reference CBBCT with 40×30 cm detector with no lateral offset

Diameter (d)	$f_g = 0.01$	$f_g = 0.15$	$f_g = 0.5$	$f_g = 1$
$d = 8$ cm	0.585	0.577	0.542	0.498
$d = 10$ cm	0.558	0.528	0.461	0.408
$d = 14$ cm	0.484	0.459	0.404	0.332
$d = 18$ cm	0.407	0.389	0.344	0.285
$d = 20$ cm	0.385	0.369	0.327	0.245

3.4. DgN^{CT} for 5 cm offset-detector CBBCT

Table 2 summarizes the DgN^{CT} values for the offset-detector geometry using a 30×30 cm detector with 5 cm lateral offset or shift. The coefficient of variation from 5 Monte Carlo runs for $d = 8$ cm and $f_g = 0.01$ was 0.14%. Comparing Tables 1 and 2, the DgN^{CT} values are nearly identical (±0.24%) for $d \leq 14$ cm. Also, the difference in DgN^{CT} between the reference and offset geometries are larger for the 20 cm breast than the 18 cm breast, as the proportion of the breast volume irradiated by the primary beam is smaller for the 20 cm diameter breast than the 18 cm diameter breast. These trends are consistent with theoretical expectations stated earlier. For the 18 cm and 20 cm diameter breasts, the percent reduction in DgN^{CT} with offset geometry computed as per Eq. 5 were 6.4% (range: 6.1% – 6.7%) and 9.6% (range: 9.4% – 9.8%), respectively, compared to reference geometry and did not show a noticeable dependence on f_g (Fig 6).

Table 2. DgN^{CT} for offset-detector CBBCT with 30×30 cm detector and 5 cm lateral offset. The COV from 5 Monte Carlo runs for the smallest breast ($f_g = 0.01$) was 0.14%.

Diameter (d)	$f_g = 0.01$	$f_g = 0.15$	$f_g = 0.5$	$f_g = 1$
$d = 8$ cm	0.581	0.574	0.543	0.499
$d = 10$ cm	0.557	0.527	0.462	0.409
$d = 14$ cm	0.482	0.459	0.404	0.332
$d = 18$ cm	0.382	0.363	0.322	0.267
$d = 20$ cm	0.349	0.333	0.296	0.221

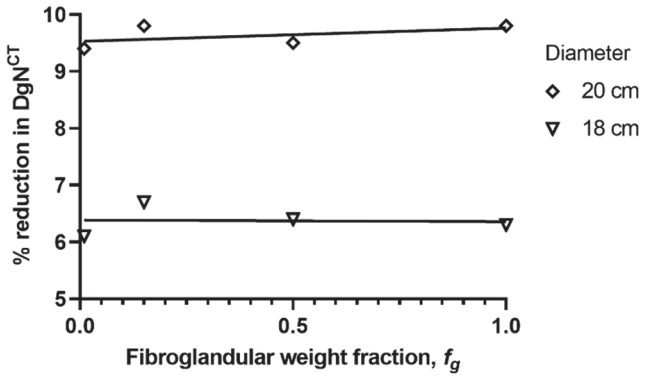

290 *Fig 6. The percent reduction in DgN^{CT} with 5 cm lateral offset with respect to reference geometry. For 1 cm to 14 cm diameter breasts the DgN^{CT} with the 5 cm lateral offset-detector geometry and the reference geometry were nearly identical* (±0.24%). Hence, *percent reduction in DgN^{CT} for 18 cm and 20 cm diameter breasts are shown. The plot indicates that the percent reduction increases with breast diameter and did not show a noticeable trend with the fibroglandular weight fraction, f_g.*

295

3.5. DgN^{CT} for 10 cm offset geometry

Table 3 summarizes the DgN^{CT} values for the offset-detector geometry using a 30×30 cm detector with 10 cm lateral offset or shift. The coefficient of variation from 5 Monte Carlo runs for $d = 8$ cm and $f_g = 0.01$ was 0.21%. Comparing Tables 1 and 3, the DgN^{CT} values are different for all breast
300 diameters, and the difference in DgN^{CT} increases with increasing breast diameter. These observations are consistent with theoretical expectations stated earlier. The percent reduction in DgN^{CT} with the 10 cm offset geometry computed as per Eq. 5 varied from 1.4% for $d = 8$ cm to 27.6% for $d = 20$ cm and is plotted in Fig 7. The plots indicate that the percent reduction in DgN^{CT} do not depend on f_g.

305 *Table 3. DgN^{CT} for offset-detector CBBCT with 30×30 cm detector and 10 cm lateral offset. The COV from 5 Monte Carlo runs for the smallest breast ($f_g = 0.01$) was 0.21%.*

Diameter (d)	$f_g = 0.01$	$f_g = 0.15$	$f_g = 0.5$	$f_g = 1$
$d = 8$ cm	0.574	0.567	0.536	0.494
$d = 10$ cm	0.518	0.491	0.429	0.379
$d = 14$ cm	0.398	0.379	0.334	0.274
$d = 18$ cm	0.304	0.291	0.258	0.214
$d = 20$ cm	0.279	0.266	0.237	0.177

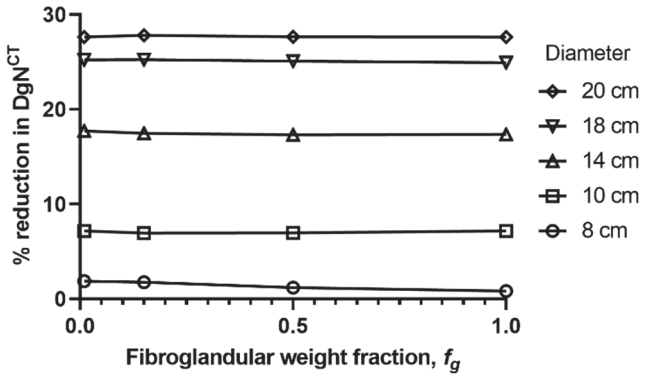

Fig 7. The percent reduction in DgN^{CT} with 10 cm lateral offset with respect to reference geometry. The plot indicates that the percent reduction increases with breast diameter and did not depend on the fibroglandular weight fraction, f_g.

3.6. Numerical fitting of DgN^{CT}

The fit equations computed from this study for the reference geometry with no lateral offset ($\alpha = 0$) and for the offset-detector geometry ($\alpha \neq 0$) are:

$$\left.\begin{aligned} DgN^{CT} &= k_0 + k_1 \times \ln(d) + k_2 \times \ln(l) + k_3 \times f_g;\ \text{when } \alpha = 0 \\ DgN^{CT} &= k_0 + k_1 \times \ln(d) + k_2 \times l + k_3 \times f_g;\ \text{when } \alpha \neq 0 \end{aligned}\right\} \quad (6)$$

It is relevant to note that the fit equation in Eqn. 6 provided for the reference geometry ($\alpha \neq 0$) is consistent in functional form with the prior report[27]. The fit coefficients and the fit statistics are summarized in Table 4. The results from the linear regression of the DgN^{CT} values derived from the fit and the values from Monte Carlo simulations are shown in Fig 8. Overall, excellent agreement is observed ($r^2 > 0.985$). The estimate ± standard error of the slope and intercept spanned unity and zero, respectively.

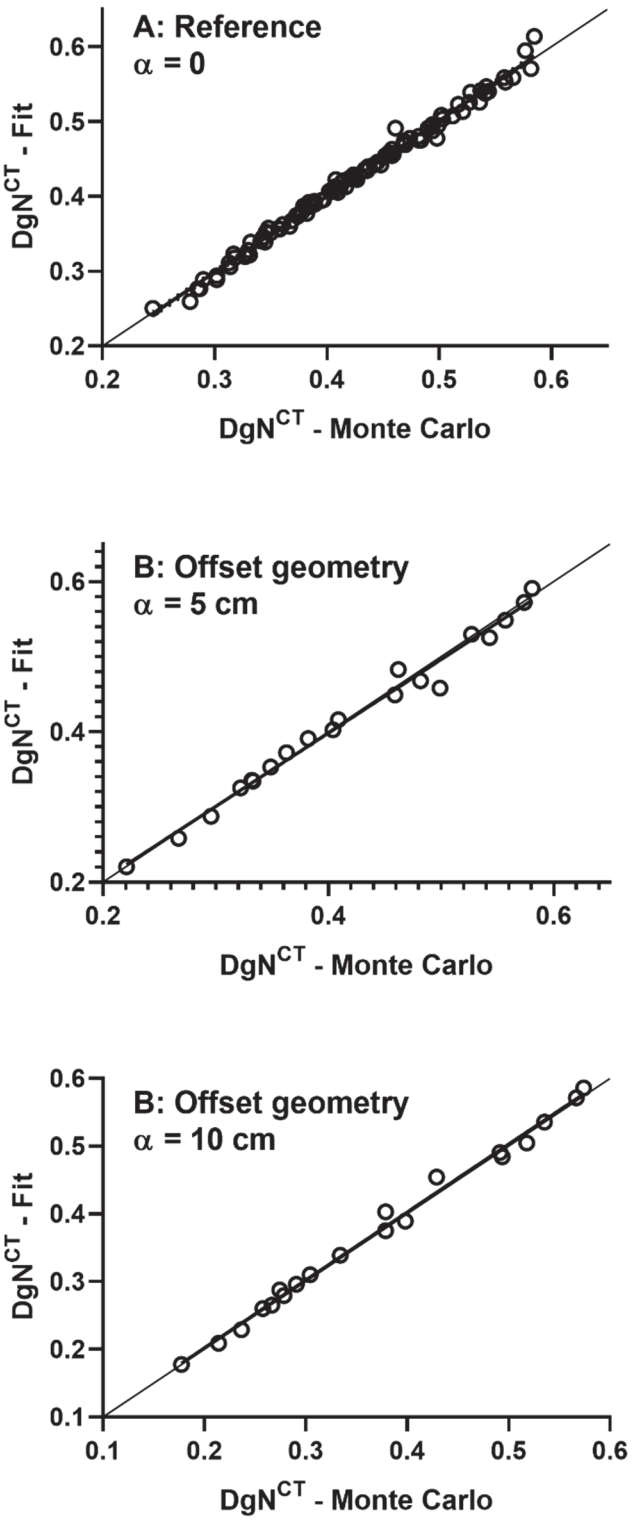

Fig 8. Linear regression of the DgN^{CT} values from the numerical fit and from Monte Carlo simulations. (a) reference geometry with no lateral-shift or offset, $\alpha = 0$; (b) offset-detector geometry with $\alpha = 5$ cm lateral-shift; and, (c) offset-detector geometry with $\alpha = 10$ cm lateral shift.

Table 4. Summary of fit coefficients in Eq. 6 and fit statistics.

	Reference CBBCT 40×30 cm detector with no offset ($\alpha = 0$)	CBBCT with 30×30 cm detector and $\alpha = 5$ cm lateral offset	CBBCT with 30×30 cm detector and $\alpha = 10$ cm lateral offset
Fit coefficients			
k_0	1.1431493495	0.8057019101	1.4174487688
k_1	-0.2904641878	-0.0375105943	-0.4263468063
k_2	0.0425061136	-0.0225960642	0.0093467709
k_3	-0.1375396676	-0.1338513840	-0.1025653286
Fit statistics			
r^2	0.9918	0.9856	0.9933
Slope ± SE	1.01375 ± 0.00887	0.97781 ± 0.02783	1.00287 ± 0.01943
Intercept ± SE	-0.00558 ± 0.00380	0.00724 ± 0.01200	0.00145 ± 0.00757
Average error [%]	0.034%	0.479%	-0.584%

4. Discussion

This study was motivated by our ongoing work on clinically translating laterally-shifted CMOS detector based CBBCT. From the lateral width of the detector ($W = 30$ cm), the largest breast diameter reported in literature ($d_{max} = 20.5$ cm) and the system magnification ($M = 1.382$), it can be inferred that the inequality in Eq. 4 is satisfied even when the detector is not laterally-shifted, i.e., $\alpha = 0$. This implies that the largest breast can be imaged without laterally-shifting the detector, provided the cross-section of the breast is circular. In reality, individual breasts may substantially deviate from circular cross-section and the lateral extent will be larger in some projection views. Also, the ability to visualize the axillary region and the lymph nodes in the lower axilla is clinically important. This requires the imaged FOV to extend beyond the breast. The offset-detector geometry is designed to achieve this purpose.

For the reference geometry which is currently used in many CBBCT systems worldwide, the DgN^{CT} values and the numerical fit provided are of practical value. The measurement procedure is as follows: The air kerma (mGy) at the AOR is measured with any phantom or object. Once a breast is imaged and the reconstructions are available, then the effective diameter (d) can be computed by equating the cross-sectional area to that of a circle. The chest-wall to nipple length (l) can be determined by using the pectoralis muscle as the landmark. The fibroglandular weight fraction (f_g) can be determined through segmentation approaches described in literature. Alternatively, estimates of d and l can be obtained from scout views. It is more challenging to determine f_g from scout views due to tissue superposition. With the knowledge of d, l and f_g, the DgN^{CT} (mGy/mGy) can be determined from the fit in Eq. 6 and the fit coefficients in Table 4. The mean glandular dose (MGD) to the breast is then computed as the product of the measured air kerma and DgN^{CT}. The readers are referred to prior articles[27,39] for additional details.

In addition to x-ray spectrum, the DgN^{CT} is dependent on the x-ray source trajectory such as circular[37-39,56] and circle-plus-line[41] trajectories, and on the assumed breast model. For circular trajectories with centered detector, DgN^{CT} coefficients have been reported by various groups assuming either semi-ellipsoidal[39,41] or cylindrical breasts[37,38,56], and for various x-ray spectra. Comparison of the results from this study with prior reports using semi-ellipsoidal breast models are addressed in section 3.2.

Estimates of absorbed dose to the breast using phantoms and either radiochromic film or thermoluminescent dosimeters (TLDs) have been reported for circular[5,10] and saddle[10] trajectories and for quasi-monochromatic x-ray beam[5] and for synchroton x-ray source operating at 38 keV[57]. These studies report a range of 3.8–5 mGy. Estimates of MGD from clinical studies report a range of 7.2–13.9 mGy for non-contrast diagnostic exams[3,20,27], and 6 mGy for an average breast targeting the MGD from 2-view mammography[2]. US FDA regulations[58] based on Mammography Quality Standards Act limit the MGD from the cranio-caudal mammographic view of an average breast to 3 mGy. Since BCT replaces the standard 2-view screening mammography with a single scan, MGD of 6 mGy is considered reasonable. It is important to note that the DgN^{CT} provided in this study is not the MGD to the breast, but is to be used in conjunction with air kerma at isocenter measured without any phantom or object. For a specified x-ray spectrum, the air kerma is dependent on the tube current and this can be varied to achieve the targeted MGD for the CBBCT exam.

This study used homogenous breast models, whereas the distribution of adipose and fibroglandular tissue in real breasts is heterogeneous. The DgN^{CT} coefficients using homogenous breast models are useful for technique factors selection to provide a targeted MGD as the tissue distribution within the breast is unknown prior to breast CT. Further, studies[59-61] have shown that the homogenous approximation overestimates MGD from CBBCT on average by 5.7% to 23%, depending on x-ray spectra, and hence provides a more conservative estimate of radiation-associate risk. Future work will address the heterogeneous tissue distribution on MGD for the offset-detector CBBCT.

We also quantified the reduction in DgN^{CT} with the offset-detector geometry with respect to the clinical system (KBCT 1000, Koning Corp.) with no detector offset. The percent reduction in DgN^{CT} with the 10 cm offset-detector geometry varied from 1.4% for $d = 8$ cm to 27.6% for $d = 20$ cm. Assuming that the same technique factors are used with offset-detector CBBCT and if clinical studies indicate comparable diagnostic accuracy, then this could lead to radiation dose reduction. A clinical trial is expected to start soon.

5. Conclusions

In this study, we conducted Monte Carlo-based computer simulations to obtain the air kerma-to-mean glandular dose (MGD) conversion factors (DgN^{CT}), also referred to as normalized mean glandular dose coefficients, appropriate for the offset-detector geometry of the clinical prototype CBBCT imaging system. The DgN^{CT} values and the numerical fit to these values are provided. Also, the DgN^{CT} values and the numerical fit to these values for the clinical CBBCT system (KBCT 1000, Koning Corp.) that uses 40×30 cm detector with no offset are provided. This would be of benefit for radiation dosimetry at these installations worldwide. There also exists a potential for radiation dose reduction due to the lower values of DgN^{CT} with offset-detector geometry, provided the same technique factors as the reference geometry are used and the image quality is clinically acceptable.

Acknowledgements

This work was supported in part by the National Cancer Institute (NCI) of the National Institutes of Health (NIH) grant R01 CA199044. The contents are solely the responsibility of the authors and do not represent the official views of the NCI or the NIH.

References

1. Glick SJ, Vedantham S, Karellas A. Investigation of optimal kVp settings for CT Mammography using a Flat-panel Imager. Medical Imaging 2002: Physics of Medical Imaging; 2002.
2. Lindfors KK, Boone JM, Nelson TR, Yang K, Kwan AL, Miller DF. Dedicated breast CT: initial clinical experience. *Radiology.* 2008;246(3):725-733.
3. O'Connell A, Conover DL, Zhang Y, et al. Cone-beam CT for breast imaging: Radiation dose, breast coverage, and image quality. *AJR Am J Roentgenol.* 2010;195(2):496-509.
4. Prionas ND, Lindfors KK, Ray S, et al. Contrast-enhanced dedicated breast CT: initial clinical experience. *Radiology.* 2010;256(3):714-723.
5. Crotty DJ, Brady SL, Jackson DC, et al. Evaluation of the absorbed dose to the breast using radiochromic film in a dedicated CT mammotomography system employing a quasi-monochromatic x-ray beam. *Med Phys.* 2011;38(6):3232-3245.
6. Vedantham S, Shi L, Glick SJ, Karellas A. Scaling-law for the energy dependence of anatomic power spectrum in dedicated breast CT. *Med Phys.* 2013;40(1):011901.
7. Kalluri KS, Mahd M, Glick SJ. Investigation of energy weighting using an energy discriminating photon counting detector for breast CT. *Med Phys.* 2013;40(8):081923.
8. Vedantham S, O'Connell AM, Shi L, Karellas A, Huston AJ, Skinner KA. Dedicated Breast CT: Feasibility for Monitoring Neoadjuvant Chemotherapy Treatment. *J Clin Imaging Sci.* 2014;4:64.
9. Cole EB, Campbell AS, Vedantham S, Pisano ED, Karellas A. Clinical Performance of Dedicated Breast Computed Tomography in Comparison to Diagnostic Digital Mammography [abstract # SSA01-09]. 101st Scientific Assembly and Annual Meeting of the Radiological Society of North America (RSNA 2015); November 29 - December 4,, 2015; Chicago, IL.
10. Shah JP, Mann SD, McKinley RL, Tornai MP. Three dimensional dose distribution comparison of simple and complex acquisition trajectories in dedicated breast CT. *Med Phys.* 2015;42(8):4497-4510.
11. Shah JP, Mann SD, Tornai MP. Characterization of X-ray scattering for various phantoms and clinical breast geometries using breast CT on a dedicated hybrid system. *J Xray Sci Technol.* 2017;25(3):373-389.
12. Shi L, Vedantham S, Karellas A, Zhu L. X-ray scatter correction for dedicated cone beam breast CT using a forward-projection model. *Med Phys.* 2017.
13. Aminololama-Shakeri S, Abbey CK, Lopez JE, et al. Conspicuity of suspicious breast lesions on contrast enhanced breast CT compared to digital breast tomosynthesis and mammography. *Br J Radiol.* 2019;92(1097):20181034.
14. Shi L, Vedantham S, Karellas A, Zhu L. The role of off-focus radiation in scatter correction for dedicated cone beam breast CT. *Med Phys.* 2018;45(1):191-201.
15. Berger N, Marcon M, Saltybaeva N, et al. Dedicated Breast Computed Tomography With a Photon-Counting Detector: Initial Results of Clinical In Vivo Imaging. *Invest Radiol.* 2019;54(7):409-418.
16. Fu Z, Tseng HW, Vedantham S, Karellas A, Bilgin A. A residual dense network assisted sparse view reconstruction for breast computed tomography. *Sci Rep.* 2020;10(1):21111.
17. Shi L, Vedantham S, Karellas A, Zhu L. Library based x-ray scatter correction for dedicated cone beam breast CT. *Med Phys.* 2016;43(8):4529.
18. O'Connell AM, Karellas A, Vedantham S. The potential role of dedicated 3D breast CT as a diagnostic tool: review and early clinical examples. *Breast J.* 2014;20(6):592-605.
19. Sarno A, Mettivier G, Russo P. Dedicated breast computed tomography: Basic aspects. *Med Phys.* 2015;42(6):2786-2804.

20. Wienbeck S, Uhlig J, Luftner-Nagel S, et al. The role of cone-beam breast-CT for breast cancer detection relative to breast density. *Eur Radiol.* 2017.
21. O'Connell AM, Karellas A, Vedantham S, Kawakyu-O'Connor DT. Newer Technologies in Breast Cancer Imaging: Dedicated Cone-Beam Breast Computed Tomography. *Seminars in ultrasound, CT, and MR.* 2018;39(1):106-113.
22. Sechopoulos I. A review of breast tomosynthesis. Part I. The image acquisition process. *Med Phys.* 2013;40(1):014301.
23. Vedantham S, Karellas A, Vijayaraghavan GR, Kopans DB. Digital Breast Tomosynthesis: State of the Art. *Radiology.* 2015;277(3):663-684.
24. Zuckerman SP, Maidment ADA, Weinstein SP, McDonald ES, Conant EF. Imaging With Synthesized 2D Mammography: Differences, Advantages, and Pitfalls Compared With Digital Mammography. *AJR Am J Roentgenol.* 2017;209(1):222-229.
25. Sujlana PS, Mahesh M, Vedantham S, Harvey SC, Mullen LA, Woods RW. Digital breast tomosynthesis: Image acquisition principles and artifacts. *Clinical imaging.* 2018.
26. Vedantham S, Karellas A, Suryanarayanan S, D'Orsi CJ, Hendrick RE. Breast imaging using an amorphous silicon-based full-field digital mammographic system: stability of a clinical prototype. *J Digit Imaging.* 2000;13(4):191-199.
27. Vedantham S, Shi L, Karellas A, O'Connell AM, Conover DL. Personalized estimates of radiation dose from dedicated breast CT in a diagnostic population and comparison with diagnostic mammography. *Phys Med Biol.* 2013;58(22):7921-7936.
28. Lindfors KK, Boone JM, Nelson TR, Shah N. Initial Clinical Evaluation of Breast Computed Tomography. Paper presented at: Radiological Society of North America Scientific Assembly and Annual Meeting Program 2005 2005; Chicago, IL.
29. Yang K, Huang SY, Packard NJ, Boone JM. Noise variance analysis using a flat panel x-ray detector: a method for additive noise assessment with application to breast CT applications. *Med Phys.* 2010;37(7):3527-3537.
30. Gazi PM, Yang K, Burkett GW, Jr., Aminololama-Shakeri S, Seibert JA, Boone JM. Evolution of spatial resolution in breast CT at UC Davis. *Med Phys.* 2015;42(4):1973-1981.
31. Konstantinidis AC, Szafraniec MB, Rigon L, et al. X-ray Performance Evaluation of the Dexela CMOS APS X-ray Detector Using Monochromatic Synchrotron Radiation in the Mammographic Energy Range. *IEEE Trans Nucl Sci.* 2013;60(5):3969-3980.
32. Vedantham S, Karellas A, Emmons MM, Moss LJ, Hussain S, Baker SP. Dedicated breast CT: geometric design considerations to maximize posterior breast coverage. *Phys Med Biol.* 2013;58(12):4099-4118.
33. Vedantham S, Tseng HW, Konate S, Shi L, Karellas A. Dedicated cone-beam breast CT using laterally-shifted detector geometry: Quantitative analysis of feasibility for clinical translation. *J Xray Sci Technol.* 2020.
34. Vedantham S, Konate S, Shi L, Shrestha S, Vijayaraghavan GR, Karellas A. Dedicated cone-beam breast CT with laterally shifted CMOS detector. The 4th International Conference on Image Formation in X-ray Computed Tomography; July 18-22, 2016, 2016; Bamberg, Germany. .
35. McKinley RL, Tornai MP, Brzymialkiewicz C, Madhav P, Samei E, Bowsher JE. Analysis of a novel offset cone-beam computed mammotomography system geometry for accomodating various breast sizes. *Phys Med.* 2006;21 Suppl 1:48-55.
36. Mettivier G, Russo P, Lanconelli N, Meo SL. Cone-beam breast computed tomography with a displaced flat panel detector array. *Med Phys.* 2012;39(5):2805-2819.
37. Boone JM, Shah N, Nelson TR. A comprehensive analysis of DgN(CT) coefficients for pendant-geometry cone-beam breast computed tomography. *Med Phys.* 2004;31(2):226-235.

38. Thacker SC, Glick SJ. Normalized glandular dose (DgN) coefficients for flat-panel CT breast imaging. *Phys Med Biol.* 2004;49(24):5433-5444.
39. Sechopoulos I, Feng SS, D'Orsi CJ. Dosimetric characterization of a dedicated breast computed tomography clinical prototype. *Med Phys.* 2010;37(8):4110-4120.
40. Sarno A, Mettivier G, Di Lillo F, Tucciariello RM, Bliznakova K, Russo P. Normalized glandular dose coefficients in mammography, digital breast tomosynthesis and dedicated breast CT. *Phys Med.* 2018;55:142-148.
41. Vedantham S, Shi L, Karellas A, Noo F. Dedicated breast CT: radiation dose for circle-plus-line trajectory. *Med Phys.* 2012;39(3):1530-1541.
42. Konate S, Vedantham S, Shi L, Karellas A. Radiation dose reduction and image quality evaluation of coronal truncated projections in cone-beam dedicated breast CT [abstract]. 2013 AAPM Annual Meeting Program, Indianapolis, IN. *Med Phys.* 2013;40(6):124.
43. Sechopoulos I, Rogers DWO, Bazalova-Carter M, et al. RECORDS: improved Reporting of montE CarlO RaDiation transport Studies: Report of the AAPM Research Committee Task Group 268. *Med Phys.* 2018;45(1):e1-e5.
44. Virshup GF, Inventor; Varian Medical Systems, Inc. (Palo Alto, CA, US), assignee. X-ray tube having a focal spot proximate the tube end. US patent 8284899. 10/09/2012, 2012.
45. Tseng HW, Vedantham S, Karellas A. Cone-beam breast computed tomography using ultra-fast image reconstruction with constrained, total-variation minimization for suppression of artifacts. *Phys Med.* 2020;73:117-124.
46. Boone JM, Kwan AL, Seibert JA, Shah N, Lindfors KK, Nelson TR. Technique factors and their relationship to radiation dose in pendant geometry breast CT. *Med Phys.* 2005;32(12):3767-3776.
47. Vedantham S, Shi L, Karellas A, O'Connell AM. Dedicated breast CT: fibroglandular volume measurements in a diagnostic population. *Med Phys.* 2012;39(12):7317-7328.
48. Huang SY, Boone JM, Yang K, Kwan AL, Packard NJ. The effect of skin thickness determined using breast CT on mammographic dosimetry. *Med Phys.* 2008;35(4):1199-1206.
49. Shi L, Vedantham S, Karellas A, O'Connell AM. Skin thickness measurements using high-resolution flat-panel cone-beam dedicated breast CT. *Med Phys.* 2013;40(3):031913.
50. Wu X, Gingold EL, Barnes GT, Tucker DM. Normalized average glandular dose in molybdenum target-rhodium filter and rhodium target-rhodium filter mammography. *Radiology.* 1994;193(1):83-89.
51. Yaffe MJ, Boone JM, Packard N, et al. The myth of the 50-50 breast. *Med Phys.* 2009;36(12):5437-5443.
52. Hammerstein GR, Miller DW, White DR, Masterson ME, Woodard HQ, Laughlin JS. Absorbed radiation dose in mammography. *Radiology.* 1979;130(2):485-491.
53. Jan S, Santin G, Strul D, et al. GATE: a simulation toolkit for PET and SPECT. *Phys Med Biol.* 2004;49(19):4543-4561.
54. Jan S, Benoit D, Becheva E, et al. GATE V6: a major enhancement of the GATE simulation platform enabling modelling of CT and radiotherapy. *Phys Med Biol.* 2011;56(4):881-901.
55. *SRS-78: Catalogue of diagnostic x-ray spectra and other data* [computer program]. The Institute of Physics and Engineering in Medicine; 1997.
56. Mettivier G, Fedon C, Di Lillo F, et al. Glandular dose in breast computed tomography with synchrotron radiation. *Phys Med Biol.* 2016;61(2):569-587.
57. Mettivier G, Masi M, Arfelli F, et al. Radiochromic film dosimetry in synchrotron radiation breast computed tomography: a phantom study. *Journal of synchrotron radiation.* 2020;27(Pt 3):762-771.

58. FDA US. Mammography Quality Standards Act Regulations. Sec. 900.12 Quality standards.(e) Quality assurance-equipment (5) Annual quality control tests. In. Rockville, MD: U.S. Food and Drug Administration; 2002.
59. Sechopoulos I, Bliznakova K, Qin X, Fei B, Feng SS. Characterization of the homogeneous tissue mixture approximation in breast imaging dosimetry. *Med Phys.* 2012;39(8):5050-5059.
60. Sarno A, Mettivier G, Tucciariello RM, et al. Monte Carlo evaluation of glandular dose in cone-beam X-ray computed tomography dedicated to the breast: Homogeneous and heterogeneous breast models. *Phys Med.* 2018;51:99-107.
61. Hernandez AM, Becker AE, Boone JM. Updated breast CT dose coefficients (DgNCT) using patient-derived breast shapes and heterogeneous fibroglandular distributions. *Med Phys.* 2019;46(3):1455-1466.